Are nanoplastics able to bind significant amount of metals? The lead example

Mélanie Davranche, Cloé Veclin, Anne-Catherine Pierson-Wickmann, Hind El Hadri, Bruno Grassl, Laura Rowenczyk, Aline N. Dia, Alexandra ter Halle, Florent Blancho, Stephanie Reynaud, et al.

Accepted Manuscript

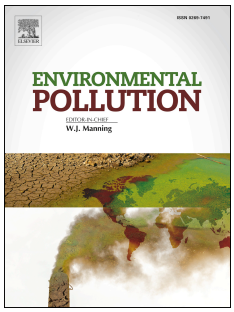

Are nanoplastics able to bind significant amount of metals? The lead example

Mélanie Davranche, Cloé Veclin, Anne-Catherine Pierson-Wickmann, Hind El Hadri, Bruno Grassl, Laura Rowenczyk, Aline Dia, Alexandra Ter Halle, Florent Blancho, Stephanie Reynaud, Julien Gigault

PII: S0269-7491(19)30540-8

DOI: https://doi.org/10.1016/j.envpol.2019.03.087

Reference: ENPO 12359

To appear in: *Environmental Pollution*

Received Date: 27 January 2019

Revised Date: 19 March 2019

Accepted Date: 21 March 2019

Please cite this article as: Davranche, Mé., Veclin, Cloé., Pierson-Wickmann, A.-C., El Hadri, H., Grassl, B., Rowenczyk, L., Dia, A., Halle, A.T., Blancho, F., Reynaud, S., Gigault, J., Are nanoplastics able to bind significant amount of metals? The lead example, *Environmental Pollution* (2019), doi: https://doi.org/10.1016/j.envpol.2019.03.087.

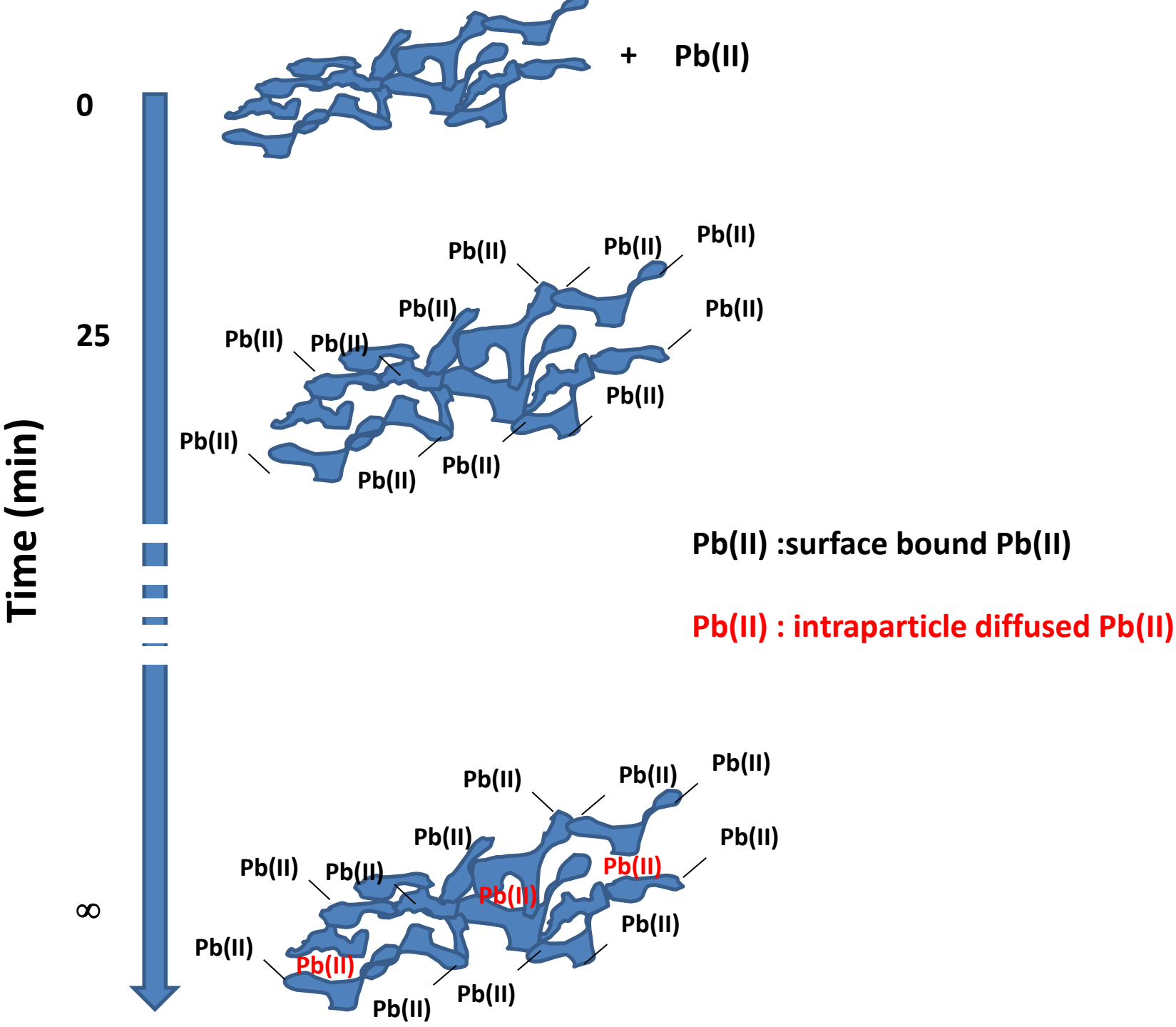
+ Pb(II)
0
25
∞
Time (min)
Pb(II)
Pb(II) :surface bound Pb(II)
Pb(II) : intraparticle diffused Pb(II)

Are nanoplastics able to bind significant amount of metals? The lead example

Mélanie Davranche[1], Cloé Veclin[1], Anne-Catherine Pierson-Wickmann[1], Hind El Hadri[2], Bruno Grassl[2], Laura Rowenczyk[3], Aline Dia[1], Alexandra Ter Halle[3], Florent Blancho[1], Stephanie Reynaud[2] and Julien Gigault[1]

[1] Univ. Rennes, CNRS, Géosciences Rennes, UMR 6118, F35000 Rennes, France

[2] IPREM, UMR 5254, CNRS-Université de Pau et des Pays de l'Adour, F64000 Pau, France

[3] Laboratoire des Interactions Moléculaires et Réactivité Chimique et Photochimique (IMRCP), UMR CNRS 5623, Université Paul Sabatier-UPS, Batiment 2R1, 3ème étage, 118, route de Narbonne, 31062 Toulouse Cedex 09, France

Corresponding author:
Mélanie Davranche
E mail: melanie.davranche@univ-rennes1.fr
Tel: +33 223 235 769
Fax: +33 223 238 787

Main finding

Nanoplastics are able to sorb high amount of Pb(II) through sorption and intraparticle diffusion processes. They could be important vector of metallic pollutant in the environment.

Highlights

- Pb(II) binding experiments onto nanoplastics extracted from environmental micro-plastics were performed.
- Pb(II) was largely bound onto nanoplastics by specific adsorption and intraparticle diffusion.
- Nanoplastics could be significant vectors of metals in the environment

Abstract

The nanoscale size of plastic debris makes them potential efficient vectors of many pollutants and more especially of metals. In order to evaluate this ability, nanoplastics were produced from microplastics collected on a beach exposed to the North Atlantic Gyre. The nanoplastics were characterized using multi-dimensional methods: asymmetrical flow field flow fractionation and dynamic light scattering coupled to several detectors. Lead(II) adsorption kinetics, isotherm and pH-

edge were then carried out. The sorption reached a steady state after around 200 min. The maximum sorption capacity varied between 97% and 78.5 % for both tested Pb concentrations. Lead(II) adsorption kinetics is controlled by chemical reactions with the nanoplastics surface and to a lesser extent by intraparticle diffusion. Adsorption isotherm modeling using Freundlich model demonstrated that NPG are strong adsorbents equivalent to hydrous ferric oxides such as ferrihydrite (log $K_{ads}^{freundlich}$ = 8.36 against 11.76 for NPG and ferrihydrite, respectively). The adsorption is dependent upon pH, in response to the Pb(II) adsorption by the oxygenated binding sites developed on account of the surface UV oxidation under environmental conditions. They could be able to compete with Fe or humic colloids for Pb binding regards to their amount and specific areas. Nanoplastics could therefore be efficient vectors of Pb and probably of many other metals as well in the environment.

Keywords.

nanoplastics, Pb(II), adsorption, kinetics, DLS, A4F

Main finding

Nanoplastics are able to sorb high amount of Pb(II) through sorption and intraparticle diffusion processes. They could be significant vectors of metallic pollutants in the environment.

1. Introduction

Due to the exceptional properties of plastics materials such as their low density and high durability, the industrial production of plastics has intensely and exponentially grown since 1940s. The reason of their success is explained by their multiples uses (e.g. food packaging, building, transport, agriculture, etc.). However, these properties result also in their exceptional persistence in the environment. Whereas marine pollution by plastics was the most highlighted (low et al., 2010; Eriksen et al., 2014), microplastic contamination of freshwater, urban water, urban dust, flood plain

soil and atmosphere were also pointed out in several studies (Gaspery et al., 2014; Dris et al. 2016; Dehghani et al., 2017; Scheurer and Bigalke, 2018; Dris et al. 2018).

Among plastic contaminants, microplastics have been the most studied (Andrady, 2011; Wright et al., 2013). However, the existence of nanoplastics, was quite recently demonstrated by Ter Halle et al. (2017) and Gigault et al. (2018). They defined nanoplastics as particles unintentionally produced, whose size was varying from 1 to 1000 nm and displaying a colloidal behavior (Gigault et al., 2018). They are produced from the use of manufactured objects but especially from aged-microplastics in response to the photo-, chemical and physical degradation mechanisms that take place under environmental conditions (Bouwmeester et al., 2015; Ter Halle et al., 2017). Their occurrence was demonstrated under laboratory conditions from degradation of plastics items (Lambert and Wagner, 2016), environmental microplastics collected in seawater (Gigault et al., 2018) and under environmental conditions in seawater samples (Ter Halle et al., 2017).

Nanoplastics display a nanoscale size. They are polydisperse with an open structure and a heterogeneous and asymmetrical shape. They present an inhomogeneous charged surface and they are able to aggregate relative to the environmental physico-chemical conditions (Gigault et al., 2018). All these properties make them formidable potential adsorbents of contaminants and especially of trace metals. However, regards to their extremely recent highlighting, no studies have ever been interested in their ability to bind trace metals and the involved governing mechanisms. Nevertheless, several studies demonstrated that both plastics pellets collected from beaches and micro-plastics recovered from seawater of the North Alantic gyre contain very variable amounts of trace metals (e.g. Holmes et al., 2012; Turner and Holmes, 2015; Vedolin et al., 2018; Prunier et al., 2019). This trace metal loading could result of the use of trace metals as additives in the plastics production and also in sorption processes (Massos and Turner, 2017; Wang et al., 2017; Prunier et al. 2019). Wang et al. (2017) suggested that the majority of metals carried by microplastics were derived from internal load. However, Holmes et al. (2014) compared the sorption capacity of virgin pellets and pellets collected from beaches. They provided evidence that trace metal adsorption was considerably

greater for the beach-sourced pellets. They attributed these results to the pellets weathering and to the resulting specific adsorption onto charged mineral sites or to non-specific interaction between the hydrophobic surface and the neutral or organic trace metal species. Adsorbed trace metals were both cations and oxyanions. Ashton et al., (2010) suggested also that trace metals may co-precipitate with or be sorbed onto hydrous oxides present onto the microplastic surface. Brennecke et al. (2016) studied the sorption of Cu and Zn from antifouling paint onto virgin polystyrene (PS) pellets and environmental aged polyvinyl chloride (PVC) fragments. They demonstrated that sorption of Cu was higher onto aged PVC than virgin PS in response to the PVC higher surface aera and polarity.

In such context, the nano size of the nanoplastics and their exceptional surface properties (charge and asymmetrical shape) make them better vectors of trace metals than pellets and microplastics. Their precise role in trace metal transfer and the involved mechanisms have therefore to be elucidated.

For this purpose, we studied the sorption of Pb(II) onto 'model' nanoplastics obtained from physical alteration of 'environmental' nanoplastics produced by sonication of microplastics collected on a beach exposed to the North Atlantics gyre in Guadeloupe (France). Lead was chosen regards to its high affinity for surface and to its toxicity. We developed an *in situ* polarography method allowing performing adsorption kinetics, isotherm and pH-sorption edge experiments in a single reactor. The evolution of the nanoplastic size and aggregation were monitored throughout the experiment using dynamic light scattering (DLS).

2. Materials and methods

All used chemicals were of analytical grade. The solutions were prepared with ultrapure water (Milli-Q system, Millipore). The containers used were (i) trace-metal cleaned with 10% (v/v) HNO_3 for 24 h at 45°C, (ii) soaked in and then rinsed with ultrapure water for 24 h at 45°C, and (iii) finally dried at 30°C. All solutions were prepared with ultrapure water (18.2 Ω, MilliQ, Millipore). The Pb(II) solutions were prepared using a 1000 mg L^{-1} standard solution of Pb $(NO_3)_2$ (standard Metrohm

99.5% ion, VWR Chemicals). The analysis of Pb^{2+} in solution was carried out by polarography (Metrohm 884 professional voltammetric meter).

2.1. Nanoplastics production

Environmental nanoplastics were produced by the sonication of 58 g of microplastics (5 mm to 2 cm) in 300 mL of ultrapure water. Sonication was performed during 5 days. The suspension was filtrated at 0.8 µm (Sartorius). Microplastics were collected in 2017 on the beach of Baie Sainte-Marie in Guadeloupe (France), which is exposed to the North Atlantic gyre. This sample corresponding to Guadeloupean nanoplastics was called NPG. Microplastics were isolated from the sand by a sea water extraction method relative to their density. Dynamic light scattering (DLS) displayed that both samples were poly-dispersed with an average hydrodynamic diameter 150-450 nm. Zeta-potential analysis demonstrated that they are negatively charged on the 2-to-14 pH range. At pH 6, zeta-potential was equal to -30.2 mV. Their final concentration in the suspension was determined by measuring the dissolved organic carbon (DOC). The NPG sample displayed a DOC concentration of 50 mg L^{-1}. Note that it cannot be excluded that a few amount of the measured DOC corresponds to organic matter.

2.2. Adsorption experiments

Kinetic experiments. Kinetic experiments of Pb(II) adsorption onto NPG were performed *in situ*, namely directly in a polarographic cell. This *in situ* methodology avoids any external treatment of the sample, Pb^{2+} concentration being continuously measured in the cell. Ten ml of the NPG solution were introduced in a polarographic cell. The pH of the NPG suspensions was fixed at 7 using HNO_3 and/or NaOH at 0.1 M and their ionic strength was fixed at 10^{-2} mol L^{-1} using KCl. Before adding Pb(II), a first polarographic measurement was performed to check (if any) the Pb^{2+} concentration release by NPG. Then, Pb(II) was added to obtain a concentration of 2 and 6 mg g^{-1} (g of dissolved organic carbon, DOC). The concentration of Pb^{2+} in the suspension was measured every 2 min during 5 h.

Adsorption isotherms. They were carried out *in situ* directly in a polarographic cell. Ten ml of the NPG solution was introduced in a polarographic cell. The pH of the NPG suspensions was fixed at 7 using HNO_3 and/or NaOH at 0.1 M. The ionic strength was fixed at 10^{-2} mol L^{-1} using KCl. Before adding Pb(II), a first polarographic measurement was performed to check (if any) the initial Pb^{2+} concentration. Then, Pb(II) was added every 4h (as assessed by the steady state) in order to obtain Pb(II) total concentration of 4, 8, 12, 16, 20 and 24 mg g^{-1} (g of DOC). The Pb^{2+} concentration was measured by polarography.

pH-adsorption edge experiment. This experiment was carried out *in situ* directly in a polarographic cell and not as classically performed in distinct batches. Fifteen mL of NPG solution were introduced in a polarographic cell. Its initial pH was fixed at 2 using HNO_3 at 0.1 M. The ionic strength was fixed at 10^{-2} mol L^{-1} using KCl. Lead(II) was added in order to obtain a concentration of 6 mg g^{-1} (g of DOC). After 4h, the Pb^{2+} concentration was measured by polarography. Then, every 4 h, the pH was increased using an automatic titrator in SET mode (Titrino 719, Metrohm). The pH was successively fixed at 3, 4, 5, 6 and 9. The Pb^{2+} concentration was measured at steady state for each pH.

2.3. Chemical Analysis

Dissolved organic carbon (DOC). DOC concentrations were determined using a Total Carbon Analyzer (Shimadzu TOC-V CSH) by a standard solution of potassium hydrogen phthalate (Sigma Aldrich). The uncertainty of the measurement was 5%.

Pb(II) measurement. Pb(II) concentrations were determined as Pb^{2+} species concentrations using polarography directly in the NPG suspensions. They were determined using a Methrohm polarogaph (Methrom 884 professional ASV) under Anodic Stripping Voltammetry (ASV) mode using a hanging dropping mercury electrode (HDME). The analytical conditions are summarized in Table S1 (supplementary file). Deoxygenation of the medium was carried out using a continuous N_2 bubbling. The analyses were carried out under stirring at 3000 rpm.

All experiments being performed directly in a polarographic cell, the metered addition method could not be carried out. A calibration curve was therefore performed for a Pb^{2+} concentration ranging in between 0 and 400 µg L^{-1}. To evaluate the impact of the NPG presence on the measurement, calibration curve were carried out with and without NPG. Moreover, to avoid any Pb(II) sorption onto NPG and ensure that all the Pb(II) was under Pb^{2+} species, the pH was fixed at 2. None influence of the NPG presence was observed. The calibration curve realized with NPG at pH 2 was therefore used to determine the experimental Pb^{2+} concentration (supplementary file Fig. S1). The detection limit of the method was 0.05 µg L^{-1} for Pb.

2.4. Nanoplastics size measurement.

Dynamic Light Scattering (DLS). DLS was used to determine the size of the nanoplastics both in the initial suspension and during the adsorption experiments. The *in situ* DLS measurements were performed using a Vasco Flex model of nanoparticle size analyzer (Cordouan Technology, Pessac, France). The probe was placed in front of the polarographic cell and measured directly in the solution. The detection limit of the DLS instrument was investigated with PSL 100 nm standards within the range of 2×10^{-5} g L^{-1} to 2×10^{-1} g L^{-1}. Although detection remains possible over the entire concentration range, an average size analysis is only possible over the concentration range of 2×10^{-2} to 2×10^{-4} g L^{-1} using the Pade-Laplace algorithm. Each measurement corresponds to a statistical average of six measurements. In addition, each of the six measurements is composed of six acquisitions of light scattered for 80 s.

Asymmetrical Flow Field Flow Fractionation (A4F) coupled to static light scattering (SLS) and inductively coupled plasma-mass spectrometry (ICP-MS). A4F-SLS-ICP-MS was used to fractionate and size sort nanoplastics with metallic composition associated to. The A4F fractionation running conditions are summarized in table S2 (supplementary file).

The detection consisted in a static light scattering (SLS, Multi Angle Light Scattering - MALS, Dawn Heleos 2, Wyatt Technology) to characterize the particles size. The incident laser wavelength of the SLS is λ=658nm. A Berry formalism that allows giving the more suitable fit of the light scattered

188 according to the angle was used. UV detector was fixed at 254 nm, which corresponds to the
189 absorption peak of the colloidal materials. Finally, an inductively coupled plasma-mass spectrometer
190 (ICP-MS 7700x, Agilent technologies) was directly coupled at the end of the detection chain without
191 using the nebulizer pump. No online quantification was performed. Here ICP-MS was used to localize
192 the Pb(II) on the colloidal size range. The ICP-MS was operated without the collision cell, because of
193 the lack of interferences for the mass isotope of interest (^{207}Pb). The sample and skimmer cones were
194 in nickel. The RF power and the plasma gas flow rate were fixed at 1500 W and 15 L min^{-1},
195 respectively.

196 **3. Results**

197 *3.1. Adsorption kinetics*

198 Lead concentration decreased extremely rapidly (Fig. 1a). After 2 min, the concentration
199 decreased from 2 to 0.43 mg g^{-1} (78.5 % of binding) and 6 to 0.17 mg g^{-1} (97.2 % of binding) for both
200 concentrations, respectively. Lead was therefore significantly adsorbed to NPG. The kinetic profile
201 consisted of a rapid adsorption following by a subsequent approach to steady state, which was
202 reached after around 200 min (Fig. 1a).

203 The kinetics was modeled using a pseudo-first-order. However, the Lagergreen pseudo-first-
204 order equation was not applicable to our Pb(II)-NPG system, no linearization of the experimental
205 data was obtained. The pseudo-second order was then tested. In this model, the rate-limiting step is
206 the surface adsorption that involves chemisorption. The model is based on the solid phase
207 adsorption capacity (Ho et al. 1996 a-b) and predicts the behavior over the whole range of
208 adsorption (Ahsu et al. 1991). The corresponding equation is:

209 $$\frac{dQ_t}{dt} = K\,(Q_e - Q_t)^2 \qquad \text{(eq.1)}$$

210 With Q_t, the adsorbed Pb(II) concentration at time t (mg g^{-1} of DOC), Q_e the adsorbed Pb(II)
211 concentration at steady state (mg g^{-1} of DOC), and K the rate constant of adsorption for the pseudo-
212 second-order (g mg^{-1} min^{-1}).

213 The integrated equation is:

$$\frac{1}{Q_t} = \left(\frac{1}{Q_e}\right).t + \frac{1}{K.Q_e^2} \quad \text{or} \quad \frac{1}{Q_t} = \frac{h}{1+ K.Q_{e.t}} \quad \text{(eq.2)}$$

Where h can be considered as the initial sorption rate. When t tends to 0, $h = KQ_e^2$

The linearity of the plots, the R^2 and the coherence between the theoretical and the experimental Qe indicated that chemical reaction is the main rate-controlling step of the binding process (Fig. 1b and Table 1). The rate constant (K) decreased with the increasing Pb(II) initial concentration as previously observed and discussed by Ho and Ofomaja (2006) and Ho et al. (2006) for Pb(II) adsorption onto palm fiber and peat.

Since the pseudo-second-order kinetic model did not allow identifying potential diffusion mechanism, the kinetic results were then analyzed using an intraparticle diffusion model. The following equation was used (El-Ashtoukhy et al., 2008):

$$Q_t = K_i.t^{0.5} + C \quad \text{(eq. 3)}$$

K_i is the rate constant of the intraparticle diffusion, whereas C corresponds to the intercept and provides information on the thickness of the boundary layer.

The Qt was plotted relative to the $\sqrt{t}$ in Fig. 1c and the kinetics parameters in Table 3. If the intraparticle diffusion model is involved the plot of Qt relative to $\sqrt{t}$ should be linear and if the intraparticle diffusion model is the rate-controlling step, the plot should pass through the origin (C = 0). However, if C ≠0, it indicates some degree of boundary layer control. The intraparticle diffusion model is therefore not the rate-controlling step, but it could operate simultaneously with other processes. The diffusion gradient can be linearized into four regions representing the external mass transfer, and the intraparticle diffusion in the macro, meso and micropore structure of the adsorbent (Allen et al., 1989; Tan et al. 2007; Ho and McKay, 1998). Multilinear lines were obtained for both initial concentrations of Pb(II) (Fig. 1c). Moreover, any of them passed through the origin indicating that the intraparticle diffusion process was not the rate-controlling step. However, the first linearity can be considered as a first step of an instantaneous adsorption or adsorption on the outer surface which was produced during the first 25 min of the sorption and corresponded to 83% and 89 % of

total bound Pb(II) for 6 and 2 mg g^{-1} initial concentration, respectively. The second part represented a more slow and progressive part of the adsorption that could be driven by an intraparticle diffusion process that limited the adsorption process and corresponded to 4% and 5 % of total bound Pb(II) for 6 and 2 mg g^{-1} initial concentration, respectively.

Therefore, Pb(II) seemed to be rapidly sorbed by a chemisorption processes which was confirmed by the pseudo-second order model parameter, that may be followed by an intraparticle diffusion process lasting up to 25 min.

3.2. Adsorption isotherm

Experimental data of the adsorption isotherm are reported in Fig. 2. The adsorbed Pb(II) concentration increased with the increasing initial Pb(II) concentration. However, the proportion of adsorbed Pb(II) was higher for the low concentration than for the high concentration, suggesting a progressive saturation of the surface.

The isotherm was fitted using the non-linear Langmuir and Freundlich models. Since no linearity was obtained for Langmuir model, Freundlich model was therefore the only model described in this work. The Freundlich isotherm assumes a multilayer sorption onto a heterogeneous surface. The Freundlich isotherm corresponds to:

$$Q_e = K_{ads} C_e^{\,n} \qquad \text{(eq. 3)}$$

Where Qe is the adsorbed Pb(II) concentration (mg g^{-1}), K_{ads} is the Freundlich adsorption constant, C_e is the concentration of Pb(II) in solution (mg g^{-1}) and n is the non-linearity coefficient.

In Fig. 2 were plotted the linearized data. Values for the Freundlich constant and coefficient are derived from the linear regression analysis of the log Qe versus log Ce. The obtained values are n= 0.34, Kads = 4.89. The correlation coefficient R^2 equal to 0.98 indicates that the Freundlich model is suitable to describe the sorption processes between Pb(II) and NPG. The coefficient n, ranging between 0 and 1, is indicative of a cooperative adsorption (here n=0.38).

These results showed that Pb(II) adsorption onto NPG was expected to be non-linear, namely produced through the formation of multilayer or through the formation of heterogeneous surface complexes. The surface complexes heterogeneity is the result of the variability of the binding sites (carboxylic, phenolic, hydroxyl, etc.) or of the denticity of the complexes (monodentates, bidentate, etc.).

3.3. pH adsorption-edge

The evolution of the Pb(II) adsorption relative to pH was non-conventionally plotted (Fig. 3). Since the experiments were both *in situ* and non-sequentially performed, it was not possible to evaluate, as done with the previous experiment, the Pb(II) concentration released by NPG at each pH. We therefore chose to present the evolution of the Pb^{2+} concentration (Fig. 3).

A Pb^{2+} concentration decrease following the increasing pH is displayed in Fig. 3. Several mechanisms could explain such result and notably the complexation of Pb(II) by the OH- ligand, whose concentration increased with the increasing pH up to the precipitation of Pb(II) as hydroxide at pH > 7. The Pb(II) speciation was calculated through VisualMinteq 3.1 considering the experimental conditions but, without NPG (Fig. 4). To allow a better comparison between the experimental and the modeled data, the Pb(II) concentration was presented in mg g^{-1} (g of DOC even if no DOC was input in the calculation, namely to convert mol L^{-1} as mg g^{-1}). Without any NPG, the modeling demonstrated that Pb^{2+} decreased from pH 6 in response to its complexation as $PbOH^{+}$ and from pH 7.5 to the precipitation of $Pb(OH)_2$s. By contrast, with NPG, Pb^{2+} decreased from pH>2, the largest decrease proceeding from pH 4. These results clearly demonstrated that the Pb^{2+} decrease was provided in response to the NPG occurrence, namely in response to the Pb^{2+} adsorption onto NPG.

3.4. Size and elemental composition characterization

DLS analysis was performed on NPG associated to Pb(II) on the studied pH range, concentrations and contact-time(kinetics) (Fig. S2, supplementary file). No significant changes were observed in the

auto-correlation function (ACF) and in the d_{zH} according to the different conditions. Nevertheless, some difference on the polydispersity could have occurred and could not be identified by DLS. The structural and physical changes of environmental nanoparticles are usually difficult to identify with DLS due to their high polydispersity in size and composition (Gigault et al., 2018). To isolate, fractionate and characterize, free-Pb(II) and Pb(II)-doped NPGs, A4F-SLS-ICPMS was further used (Fig. 5). The fractograms displayed a signal with a retention time covering the size range from 50 nm up to 400 nm (in diameter) based on A4F calibration (Gigault et al., 2017) (Fig. 5.a). The intensity of the UV signal was slightly higher for Pb(II)-doped NPG than for free-Pb(II) NPG. Such results might be produced in response to the Pb(II) adsorbed onto the NPG surface or to the NPG dispersion in presence of Pb(II). The retention time was not modified indicating no modification of the size distribution range. However, the UV signals showed a large colloidal fraction (from 10kDa to 60kDa) at a retention time t_R=2 min. Residues of polymers, additives and organic matter remaining on the microplastics surface, possibly released during the sonication. The SLS analysis validated these observations. They displayed that NPG have a gyration radius ranging from 70 to 250 nm using Berry formalism for both Pb(II)-doped and free-Pb(II) NPG. Angular dependence of the light scattered did not fit using the spherical formalism indicating an indirect shape deviating from the ideal sphere (SI, Fig. S2. The on-line coupling of ICPMS and A4F-UV-SLS allow obtaining the elemental composition associated to the UV and SLS signals (Fig. 5b). The m/z 207 trace, corresponding to Pb(II) increased from t_R=5min to t_R=17min for Pb(II)-doped NPG (black trace) as compared to free-Pb(II) NPG (blue trace) indicating that Pb(II) was associated to NPG. Noted that for free-Pb(II) NPG, the m/z 207 trace presented some spikes, starting especially at t_R=12min, namely at approximately 100 nm size. Such spiked signal corresponds to the signal generally observed with ICP-MS in single particle mode. When a significant amount is localized in a nanometer resolved surface, the quantity of ionized metal is significantly higher, which corresponds to either metal nanoparticles trapped inside colloids or metal accumulation within a cavity of a porous material. Nevertheless, for the Pb(II)-doped NPG, the spiked

signal was attenuated suggesting either, a Pb(II) surface adsorption or ,that the equilibrium time was long enough to allow a significant Pb(II) accumulation in the porosity.

4. Discussion

4.1. NPG is a significant Pb(II) adsorbent

Adsorption kinetic experiments displayed that 78.5 and 97 % of Pb(II) were sorbed onto the nanoplastics at pH 7. These proportions are high and suggest that nanoplastics are strong Pb(II) adsorbent. The Freundlich K_{ads} defined for Pb(II)-NPG in the present study was compared to the Freundlich K_{ads} of various adsorbents. For the comparison, it was necessary to recalculate our constants using the same calculation units than those of the literature. They are reported in Table 2. Since in the literature, no data exist for the Pb(II) binding to nanoplastics, our results were therefore compared to those obtained for plastics pellets collected on beaches on which Pb(II) was experimentally adsorbed using sea and river water samples (Holmes et al., 2012; 2014). Note that the beached pellets are micrometric and that they were submitted to sonication during 5 min before being used. Although pH values were close to each other, the present Freundlich K_{ads} is 3 to 4 order of magnitude higher than those of beached pellets (Table 2). The environmental nanoplastics (NPG) are therefore stronger Pb(II) adsorbent than environmental micrometrics plastics. Note however, that the sonication step submitted to the beached pellets could have released many nanometric parts decreasing thus their binding capacity. Regards to these results, the present Freundlich K_{ads} was compared to the K_{ads} calculated for Pb(II) binding to minerals known to be strong metals adsorbents, namely the Fe oxyhydroxides. First, K_{ads} was compared to those calculated for Pb(II)-goethite sorption. Goethite is a well-crystallized Fe oxyhydroxides with a low specific surface around 45 g m^{-2}. The present Freundlich K_{ads} was 1 or 2 orders of magnitude higher than those of goethite (Table 2). However, the binding experiments of Pb(II) to goethite were performed at lower pH. The metal sorption onto Fe oxyhydroxides being strongly dependent to pH, the difference noted in between the Freundlich K_{ads} could be involved by this pH difference, see notably the Olu-Owolabi and Ajayi (2011)

study where pH was 4.2. By contrast, Freundlich K_{ads} of Pb(II)-ferrihydrite sorption is in the same order of magnitude than the present K_{ads}. Ferrihydrite is a Fe oxyhydroxide with a high specific surface varying between 250 to 600 g m^{-2} and is considered to be the strongest metal sorbent amongst various particulate Fe oxyhydroxides. The similarity of the ferrihydrite and the present Freundlich K_{ads} therefore suggests that NPG are strong adsorbent of Pb(II). Finally, the Freundlich K_{ads} was compared to that obtained for nano-goethite, to eventually identify the role of the nano-size on the sorption. Both Freundlich K_{ads} are in the same order of magnitude although they were highly different for particulate goethite. Finally, our data were compared to that obtained for a purified humic acid (PPHA). The Freundlich K_{ads} was calculated from data extracted from the Pb-humic acid data compilation performed by Milne et al., (2001). Freundlich isotherm was not able to model Pb-humic acid binding data except that of Pinheiro et al. (1994), the Langmuir isotherm providing better modeling. Regarding the pH conditions, we can consider that both Freundlich K_{ads} are in the same order of magnitude.

All these comparisons demonstrated that NPG are strong adsorbent of Pb(II), much stronger than beached micrometric plastics pellets. Their sorption capacity seems to be similar to strong metal sorbent such as ferrihydrite, nano-goethite and humic acid. Their sorption properties can thus be attributed to their nano-size and subsequent high specific surface area such as those of ferrihydrite, nano-goethite and humic acid.

4.2. Mechanisms involved in Pb(II) adsorption

We demonstrated that NPG is a strong adsorbent of Pb(II). Let us go further to elucidate which are the mechanisms involved in the Pb(II) binding to NPG.

The first interesting results are provided by the adsorption kinetic study. The kinetic rate could not be modeled using the pseudo first-order model demonstrating that the adsorption kinetics was not controlled by the diffusion. By contrast, the pseudo-second order model allowed with success to model the kinetic data, indicating that the major rate limiting step was the surface adsorption involved by chemical interactions in between Pb(II) and NPG. Although this process dominates the

adsorption, intraparticle diffusion seems also to partly control the mechanism of Pb(II) adsorption onto NPG.

Lead(II) sorption onto NPG was strongly dependent to pH as shown by the pH-adsorption-edge experiment (Fig. 3). With the increasing pH, the surface electronegativity increased in response to the surface functional groups deprotonation. In such conditions, Pb(II) affinity for the surface increased, Pb(II) being able to be bound through electrostatic interactions (outer sphere complex) and/or covalent binding (inner sphere complex). The formation of inner spheres supposes the presence of surface sites able to exchange electron such as, hydroxyl, carboxylic and phenolic functional sites. Figure 3 shows that Pb^{2+} concentration strongly decreased from pH > 4 (i.e. Pb(II) adsorption strongly increased). This pH corresponds to pH from which carboxylic groups generally become significantly deprotonated ($pKa_{R\text{-}COOH} \approx 4.8$). If no data are available for nanoplastics, several studies showed that plastics debris collected on beach or seawater displayed a higher oxidation state than the reference sample (Ter Halle et al., 2017). Fourier Transform Infra-red Spectroscopy (FTIR) of weathered plastics showed that oxygenated moieties such as, aldehydes, ketones, alcohol, hydroperoxides and carboxylic acids groups increase in the plastics with the duration exposure (Andrady, 2017). The increase of the oxygen moieties and oxygenated function is involved by the UV irradiations weathering. The modeling of the adsorption isotherm data with the Freundlich model demonstrated that the adsorption was not only favorable but, heterogeneous in response to either a multilayer sorption or the formation of heterogeneous surface complexes (surface sites and complex denticity heterogeneity). Since Pb(II) is a transition metal whose potential to form covalent binding is high, the multilayer binding is therefore unlikely. However, regarding the oxidation state of the NPG surface, the formation of heterogeneous complexes with various sites such as, carboxylic, hydroxyl or phenolic sites is more than expected. Note, however, that Pb(II) sorption onto NPG surface does not affect the aggregation/dispersion of the NPG, since no difference in their size and Rg variation was observed with or without Pb(II).

As previously explained, fractograms of free Pb(II) and Pb(II)-doped NPG obtained with A4F-ICPMS, exhibited spikes in the R_g range over 100 nm. Passing 100 nm in R_g, the frequency of high-intensity spikes increases. Nevertheless, the present A4F-ICPMS set up is not optimized to characterize nanoparticle size using the single particle-ICPMS mode (Schwertfeger et al., 2016; Bustos and Winchester, 2016). Dwell and settling times are not indeed sufficient to obtain a robust correlation between the intensity of the spike and the exact size distribution. These spikes and single-particle event in the fractograms could be explained by the absorption and accumulation of Pb(II) in the NPG structure/porosity, confirming the intraparticle diffusion of Pb(II). Note that the Pb(II) occurring in the porosity and in the residual structure of the free-Pb(II) NPG are strongly trapped since very fewly released at acidic pH as shown by the polarographic measurements. The number and intensity of spikes was higher for free-Pb(II) than for Pb(II)-doped NPG in response to the Pb(II) adsorption in high proportion onto the NPG surface that partly hid the spike signal. Such result confirms the large surface adsorption of Pb(II) to NPG as previously evidenced by experimental data and modeling.

All this results demonstrated that Pb(II) is adsorbed on the NPG in high amount through its binding as surface complexes with the oxygenated binding sites produced by the UV irradiation under environmental conditions. This major process is, however, coupled to a physical trapping/concentration of Pb(II) in the structure/porosity of the largest NPG in response to an intraparticle diffusion mechanism.

4.3. Is this sorption mechanism environmentally significant?

The present results clearly demonstrate that nanoplastics have strong affinity for metals. The question becomes then to identify whether this affinity could impact significantly the metal environmental fate. The answer depends on two major parameters: (i) the nanoplastics environmental amount and (ii) their ability to compete with the other significant metal ligands such as, Fe(III) nano-oxides and/or organic matter.

No thorough quantitative information exists on the true amount of nanoplastics occurring in the environment. However, hypotheses regarding their presence within environment allow some estimations to be performed as follows. Although across the oceans, the total mass of microplastics was estimated, using circulation models, to vary in between 9.3 to 23.6 10^3 tons, only 1% of this estimated amount is actually found in the ocean (Jambeck et al., 2015). Several authors suggested that this difference could be explained by the alteration of the micro-plastics as nanoplastics in response to the ultraviolet radiation, physical wave forces and hydrolysis in ocean (Andrady et al., 2011; Gigault et al., 2016; Ter Halle et al. 2017). If nanoplastics would be equally distributed in the whole ocean water (liquid water), their hypothetic concentration would vary from 7 to 18 pg L^{-1}, which is rather low. However, accumulation zones of microplastics have been identified in several regions such as, Artic water or oceanic gyres where microplastics can exceed $6x10^5$ pieces km^{-2}, which represent for the average depth of oceans 2.3 $x10^{18}$ pieces L^{-1} (Law et al., 2010; Bergman et al., 2016, Peeken et al. 2018). Considering that these microplastics represent 1% of the plastics present in ocean, the nanoplastics amount in such samples can potentially reach 2.3 10^{20} pieces L^{-1} which is rather high. In soils, the quantitative occurrence of microplastics and nanoplastics are considered as scarce and inexistant, respectively (Rillig et al., 2012). However, the plastic particle loading in agroecosystems should be high due to inputs of both recycled organic wastes and plastic film mulching (Ng et al., 2018). Therefore, in some specific worldwide microplastic accumulation areas, nanoplastics concentrations could be significant making them alternative actors to be considered in the metal cycles and accumulation.

Concerning their ability to compete with strong soluble or solid ligands for metal binding a first answer can be found in Table 1. The Freundlich K_{ads} compilation indeed demonstrates that for equivalent mass, the Freundlich K_{ads} being in the same order of magnitude, nanoplastics could be potential competitors for Fe nano-oxides and humic substances. However, this competition will depend on the specific area and the binding sites density between the competitive ligands and the nanoplastics. Finally, the key points to be considered before starting regarding such competition are

441 the interactions that could be performed between these ligands and the nanoplastics (aggregation,
442 coating, repulsion, etc.). These interactions could, indeed, increase the potential of nanoplastics to
443 bind metals (through additive effects) or by contrast limit their sorption capacities by recovering their
444 surface limiting as a consequence their binding sites availability.

445 **5. Conclusion**

446 Nanoplastics, recently identified and characterized, are emerging pollutants. Their size makes
447 them potential vectors of other pollutants such as metals. This study provided evidence that
448 nanoplastics, formed in natural conditions under which they are mechanically degraded and
449 especially oxidized by UV irradiations, are able to adsorb Pb(II). Lead(II) adsorption seems to be
450 controlled by chemical and physical interactions with NPG. Adsorption is strongly dependent to pH.
451 A large increase in the adsorption was evidenced for pH > 4 that corresponds to the carboxylic sites
452 deprotonation. This observation suggests that Pb(II) could be bound to the surface oxygenated
453 binding sites through inner sphere complexes, which result in an heterogeneous adsorption process.
454 To a lesser extent, sorption seems to depend on a Pb(II) intraparticle diffusion as evidenced by
455 modeling and analytical results.

456 The sorption capacity of nanoplastics are high, with Pb(II) Freundlich binding constants close to
457 those of ferrihydrite, nano-goethite and humic acid, known to be strong adsorbents of metals. If no
458 evidence were provided that microplastics are able to load high amount of metals, by contrast the
459 present study demonstrated that the nanometric size and surface properties of nanoplastics
460 produced under environmental conditions, can allow nanoplastics to be efficient vectors of Pb(II) and
461 probably of many other metals. Moreover, both modalities of Pb binding to NPG raise the question
462 of the subsequent bioavailability of the bound metals. Are adsorbed Pb(II) more available than
463 porosity trapped Pb(II) or inversely?

464

465 **Acknowledgements**

This work was supported by the ANR PRC program through the PEPSEA project coordinated by Julien Gigault.

References

Aksu, Z., 2001. Equilibrium and kinetic modelling of cadmium(II) biosorption by C. vulgaris in a batch system: effect of temperature, Separation and Purification Technology, 21, 285-294.

Allen, S.J., Mckay, G., Khader, K.Y.H., 1989. Intraparticle diffusion of a basic dye during adsorption onto sphagnum peat. Environ. Pollut., 56(1), 39-50

Andrady, A.L., 2017. The plastic in microplastics: a review. Mar. Pollut. Bull., 119(1), 12-22.

Ashton, K., Holmes, L., Turner, A., 2010. Association of metals with plastic production pellets in the marine environment. Mar. Pollut. Bull., 60(11), 2050-2055.

Bergmann, M., Sandhop, N., Schewe, I., D'Hert, D. 2016. Observations of floating anthropogenic litter in the Barents Sea and Fram Strait, Arctic. Polar biol., 39, 553-560.

Bouwmeester, H., Hollman, P. C., Peters, R. J., 2015. Potential health impact of environmentally released micro- and nanoplastics in the human food production chain: experiences from nanotoxicology. Environ. Sci technol., 49(15), 8932-8947.

Brennecke, D., Duarte, B., Paiva, F., Caçador, I., Canning-Clode, J., 2016. Microplastics as vector for heavy metal contamination from the marine environment. Estuar. Coast. Shelf Sci., 178, 189-195.

Bustos, A.R.M., Winchester, M.R., 2016. Single-particle-ICP-MS advances. 5051-5052

Christophi, C A., Axe, L., 2000. Competition of Cd, Cu, and Pb adsorption on goethite. J. Environ. Eng., 126(1), 66-74.

Dehghani, S., Moore, F., Akhbarizadeh, R., 2017. Microplastic pollution in deposited urban dust, Teheran metropolis, Iran. Environ. Sci. Pollut. Res., 24(25), 20360-20371.

Dris, R., Gasperi, J., Saad, M., Mirande, C., Tassin, B., 2016. Synthetic fibers in atmospheric fallout: a source of microplastics in the environment? Mar. Pollut. Bull., 104(1-2), 290-293.

Dris, R., Imhof, H.K., Löder, M.G., Gasperi, J., Laforsch, C., Tassin, B., 2018. Microplastic Contamination in Freshwater Systems: Methodological Challenges, Occurrence and Sources. *In* Microplastic Contamination in Aquatic Environments (pp. 51-93).

El-Ashtoukhy, E.S., Amin, N.K., Abdelwahab, O., 2008. Removal of lead (II) and copper (II) from aqueous solution using pomegranate peel as a new adsorbent. Desalination, 223(1-3), 162-173.

Eriksen, M., Lebreton, L.C., Carson, H.S., Thiel, M., Moore, C.J., Borerro, J.C., Galgani, F.,Gasperi, J., Dris, R., Bonin, T., Rocher, V., Tassin, B., 2014. Assessment of floating plastic debris in surface water along the Seine River. Environ. Pollut., 195, 163-166.

Gigault, J., El Hadri, H., Reynaud, S., Deniau, E., Grassl, B., 2017. Asymmetrical flow field flow fractionation methods to characterize subjulienmicron particles: application to carbon-based aggregates and nanoplastics. Anal. Bioanal. Chem., 409(29), 6761-6769.

Gigault, J., Pedrono, B., Maxit, B., Ter Halle, A. 2016. Marine plastic litter: the unanalyzed nano-fraction. Environ. Sci. Nano, 3, 346-350.

Gigault, J., Ter Halle, A., Baudrimont, M., Pascal, P.Y., Gauffre, Phi, T. L., El Hadri, H., Grassl, B., Reynaud S., 2018. Current opinion: What is a nanoplastic? Environ. Pollut., 235, 1030-1034.

Ho Y.S., Wase D.A.J., Forster C.F., 1996b. Kinetic studies of competitive heavy metal adsorption by sphagnum moss peat, Environ. Sci. Technol.. 17, 71–77.

Ho, Y.S., McKay, G., 1998. Kinetic models for the sorption of dye from aqueous solution by wood. Pro. Safe. Environ. Protect., 76(2), 183-191.

Ho, Y.S., Wase, D.A.J., Forster, C.F., 1996a. Removal of lead ions from aqueous solution using sphagnum moss peat as adsorbent. WATER SA-PRETORIA-, 22, 219-224.

Holmes, L.A., Turner, A., Thompson, R.C., 2012. Adsorption of trace metals to plastic resin pellets in the marine environment. Environ.l Pollut., 160, 42-48.

Holmes, L.A., Turner, A., Thompson, R.C., 2014. Interactions between trace metals and plastic production pellets under estuarine conditions. Mar. Chem., 167, 25-32.

Jambeck, J. R., Geyer, R., Wilcox, C., Siegler, T. R., Perryman, M., Andrady, A., Narayan R, Law, K. L. 2015. Plastic waste inputs from land into the ocean. Science, 347, 768-771.

Law, K. L., Morét-Ferguson, S., Maximenko, N. A., Proskurowski, G., Peacock, E. E., Hafner, J., & Reddy, C. M. (2010). Plastic accumulation in the North Atlantic subtropical gyre. Science, 329(5996), 1185-1188.

Massos, A., Turner, A., 2017. Cadmium, lead and bromine in beached microplastics. Environ. Pollut., 227, 139-145.

Milne, C. J., Kinniburgh, D. G., Van Riemsdijk, W. H., Tipping, E. 2003. Generic NICA− Donnan model parameters for metal-ion binding by humic substances. Environ. Sci. Technol., 37, 958-971.

Mohapatra, M., Mohapatra, L., Singh, P., Anand, S., Mishra, B.K., 2010. A comparative study on Pb (II), Cd (II), Cu (II), Co (II) adsorption from single and binary aqueous solutions on additive assisted nano-structured goethite. Inter. J. Eng. Sci. Technol., 2, 89-103.

Ng, E. L., Lwanga, E. H., Eldridge, S. M., Johnston, P., Hu, H. W., Geissen, V., Chen, D. 2018. An overview of microplastic and nanoplastic pollution in agroecosystems. Sci. Tot. Environ., 627, 1377-1388.

Olu-Owolabi, B.I., Ajayi, S.O., 2011. Adsorption thermodynamics of cations onto goethite and goethite-humic acid complex. J. Chem. Mat. Sci., 1, 14-24.

Peeken, I., Primpke, S., Beyer, B., Gütermann, J., Katlein, C., Krumpen, Bergmann, M., Hehemann, L., Gerdts, G. 2018. Arctic sea ice is an important temporal sink and means of transport for microplastic. Nature Com., 9, 1505.

Pinheiro, J. P., Mota, A. M., Goncalves, M. S. 1994. Complexation study of humic acids with cadmium (II) and lead (II). Analytica Chimica Acta, 284, 525-537.

Prunier, J., Maurice, L., Perez, E., Gigault, J., Pierson-Wickmann, A.C., Davranche, M., Ter Halle, A., 2019. Trace metals in polyethylene debris from the North Atlantic subtropical gyre. Environ. Pollut., 245, 371-379.

Rillig, M. C. 2012. Microplastic in Terrestrial Ecosystems and the Soil? Environ. Sci. Technol., 46, 6453-6454.

Rout, K., Mohapatra, M., Anand, S., 2012. 2-Line ferrihydrite: synthesis, characterization and its adsorption behaviour for removal of Pb (II), Cd (II), Cu (II) and Zn (II) from aqueous solutions. Dalton Transac., 41(11), 3302-3312.

Ryan, P.G., Reisser, J., 2014. Plastic pollution in the world's oceans: more than 5 trillion plastic pieces weighing over 250,000 tons afloat at sea. PloS one, 9(12), e111913.

Scheurer, M., Bigalke, M., 2018. Microplastics in Swiss floodplain soils. Environ. Sci. Technol. , 52(6), 3591-3598.

Schwertfeger, D.M., Velicogna, J.R., Jesmer, A. H., Scroggins, R.P., Princz, J.I., 2016. Single particle-inductively coupled plasma mass spectroscopy analysis of metallic nanoparticles in environmental samples with large dissolved analyte fractions. Anal. Chem., 88(20), 9908-9914.

Tan, I.A.W., Hameed, B.H., Ahmad, A. L., 2007. Equilibrium and kinetic studies on basic dye adsorption by oil palm fibre activated carbon. Chem. Eng. J., 127(1-3), 111-119.

Ter Halle, A., Jeanneau, L., Martignac, M., Jardé, E., Pedrono, B., Brach, L., Gigault, J., 2017. Nanoplastic in the North Atlantic subtropical gyre. Environ. Sci. Technol., 51(23), 13689-13697.

Vedolin, M.C., Teophilo, C.Y.S., Turra, A., Figueira, R.C.L., 2018. Spatial variability in the concentrations of metals in beached microplastics. Mar. Pollut. Bull., 129(2), 487-493.

555 Wang, J., Peng, J., Tan, Z., Gao, Y., Zhan, Z., Chen, Q., Cai, L., 2017. Microplastics in the surface sediments from
556 the Beijiang River littoral zone: composition, abundance, surface textures and interaction with heavy metals.
557 Chemosphere, 171, 248-258.

558 Wright, S.L., Thompson, R.C., Galloway, T.S., 2013. The physical impacts of microplastics on marine organisms:
559 a review. Environ. Pollut., 178, 483-492.

Table 1: Kinetic parameters calculated using the pseudo second order model and the intraparticle diffusion model for the kinetic adsorption experiment at [Pb(II)] = 2 mg g^{-1} and [Pb(II)] = 6 mg g^{-1}.

Kinetic parameters	**Kinetic experiment at [Pb(II)] = 2 mg g^{-1}**	**Kinetic experiment at [Pb(II)] = 6 mg g^{-1}**
Pseudo-second order model		
$Qe_{theorical}$ (mg g^{-1})	1.89	5.44
K (g mg^{-1} min^{-1})	0.24	0.072
h (mg g^{-1} min^{-1})	0.88	2.14
R^2	1	0.999
$Qe_{experimental}$ (mg g^{-1})	1.89	5.46
Intra-particle diffusion		
Ki_1 (mg g^{-1} $min^{-1/2}$)	0.07	0.16
C_1 (g mg^{-1} min^{-1})	1.5	4.2
R^2_1(mg g^{-1} min^{-1})	0.98	0.98
Ki_2 (mg g^{-1} $min^{-1/2}$)	0.008	0.023
C_2 (g mg^{-1} min^{-1})	1.76	5.06
R^2_2(mg g^{-1} min^{-1})	0.87	0.78

Table 2: Comparison of the present calculated Freundlich K_{ads} and the Freundlich K_{ads} of Pb(II) binding to various adsorbents.

Sample	**K_{ads}**	**K_{ads} (present study)**	**Calculation units**	**References**
Beached pellet in sea water pH= 7.8	2.1×10^{-1}	4.6×10^{2}	y: µg g^{-1} x: µg L^{-1}	Holmes et al. (2012)
Beached pellets in sea water pH= 7.8	6.5×10^{-1}	3.5×10^{3}	y: nmol g^{-1} x: nmol L^{-1}	Holmes et al. (2014)
Beached pellets in river water pH= 6.3	3.7×10^{-1}	3.5×10^{3}	y: nmol g^{-1} x: nmol L^{-1}	Holmes et al. (2014)
Goethite pH= 6, IS = 10^{-3} M	3×10^{-4}	4.5×10^{-3}	y: mol g^{-1} x: mol L^{-1}	Christophi and Axe (2000)
Goethite pH = 4.2	1.710^{-1}	1.4×10^{1}	y: mmol kg^{-1} x: µmol L^{-1}	Olu-Owolabi and Ajayi (2011)
Ferrihydrite pH = 5.5	11.76	8.31	y: mg g^{-1} x: mg L^{-1}	Rout et al. (2012)
Nano-goethite pH = 5.5	10.33	8.31	y: mg g^{-1} x: mg L^{-1}	Mohapatra et al. (2010)
Purified Humic Acid (PPHA) pH = 5	1.40	8.31	y: mg g^{-1} x: mg L^{-1}	Pinheiro et al. (1994)

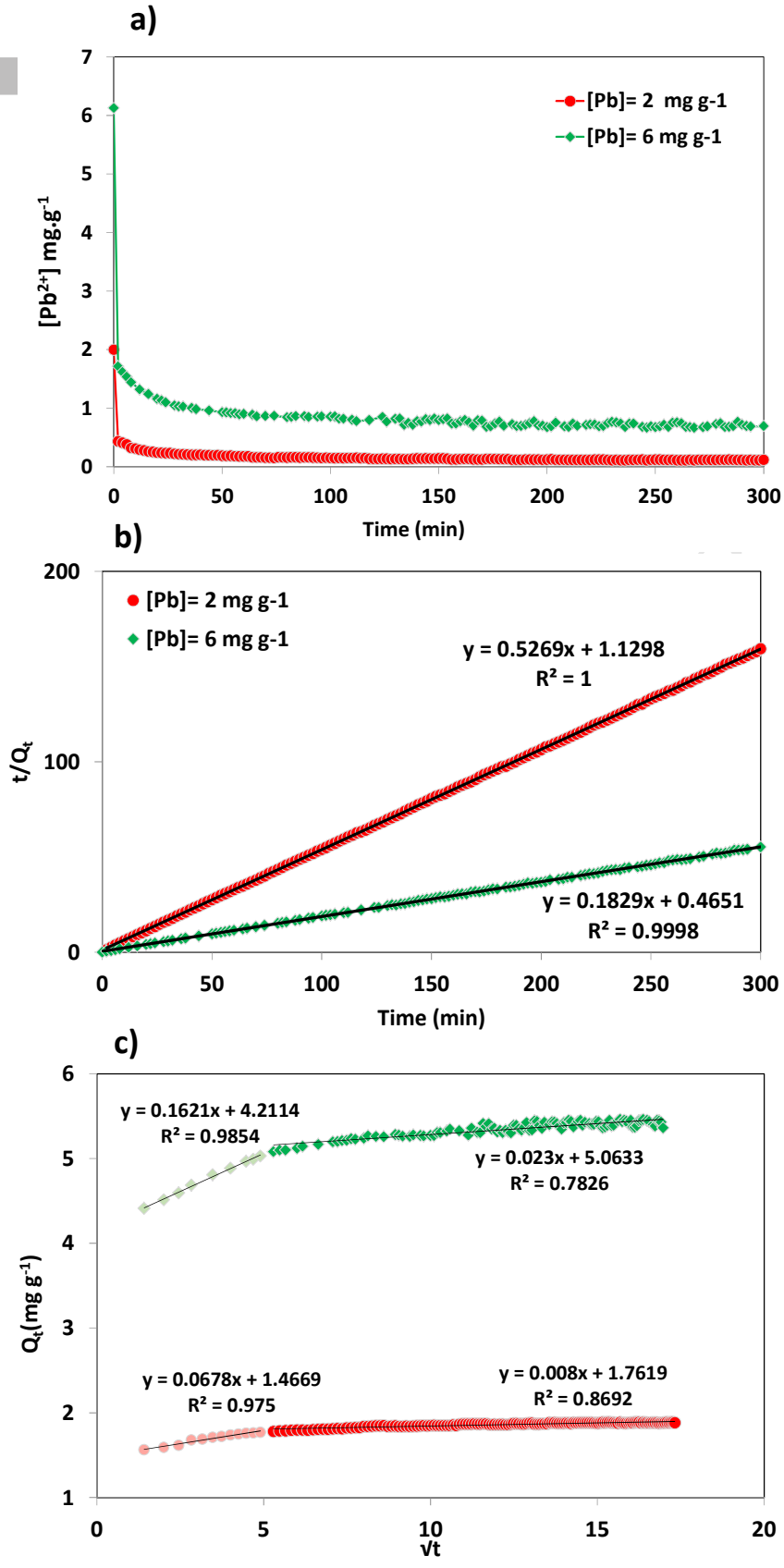

Figure 1: a) Time-dependent Pb(II) sorption onto NPG for b) Pseudo second order kinetics modelling, c)Intraparticle diffusion kinetic model for $[Pb(II)]_{initial}$=0.3 mg L^{-1} and $[Pb(II)]_{initial}$=0.1 mg L^{-1}, corresponding to red and green symbols, respectively

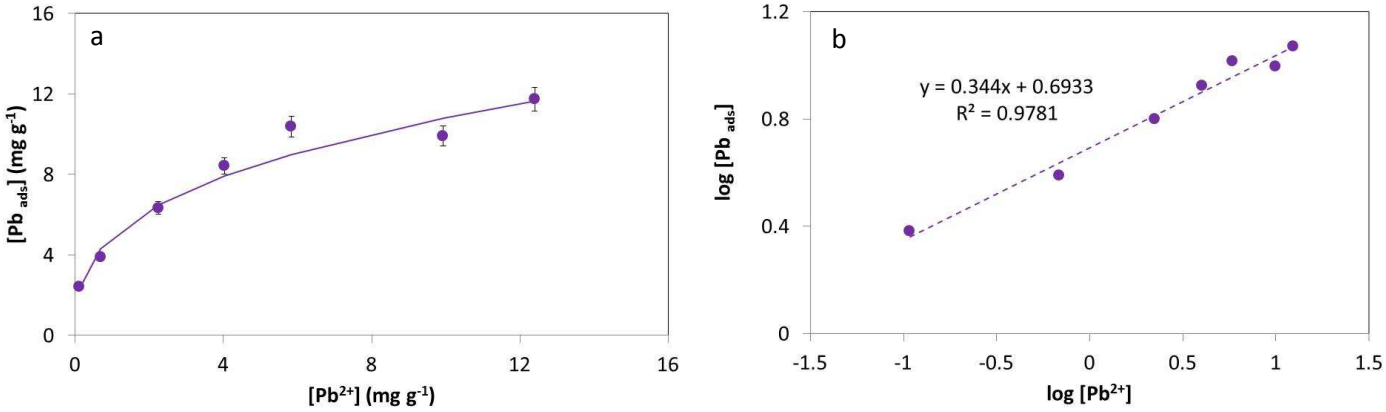

Figure 2: Adsorption isotherm of Pb(II) onto NPG at pH 7: a) experimental and modeled data and b) linearization of the experimental data using the Freundlich model.

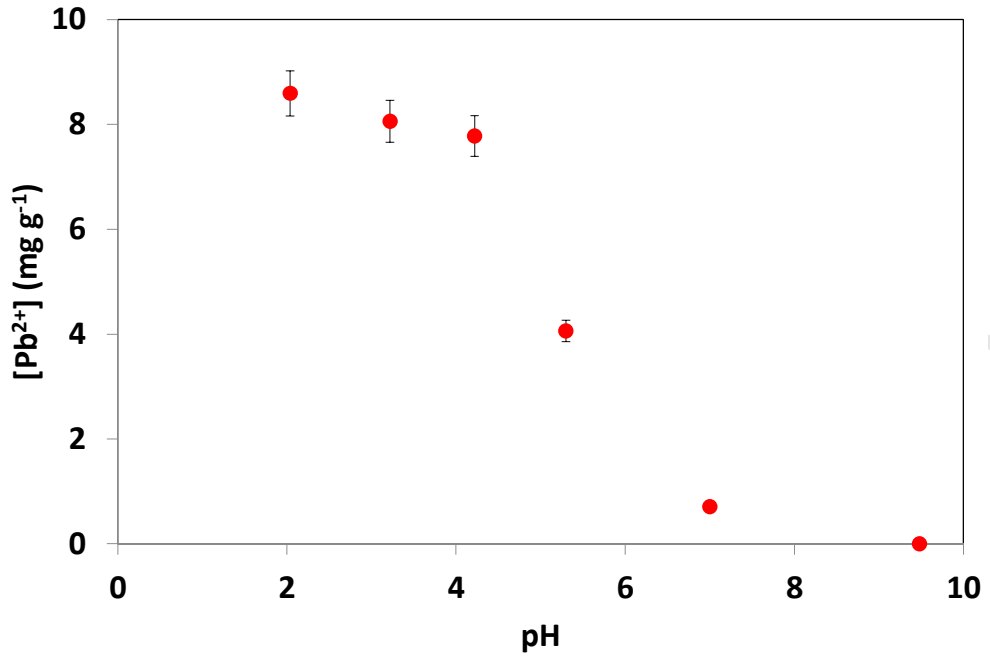

Figure 3: Evolution of the Pb^{2+} concentration relative to pH in presence of NPG at 50 mg g^{-1}.

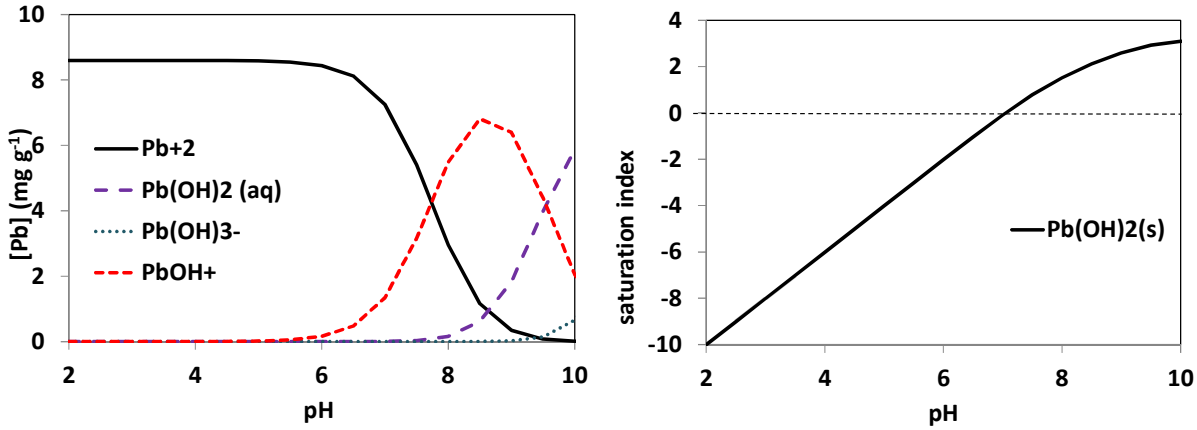

Figure 4: Pb(II) speciation under pH-adsorption-edge experimental condition but without NPG: a) corresponds to the Pb^{2+} speciation in solution and b) the evolution of the saturation index of $Pb(OH)_2s$, the unique species that was identified to precipitate.

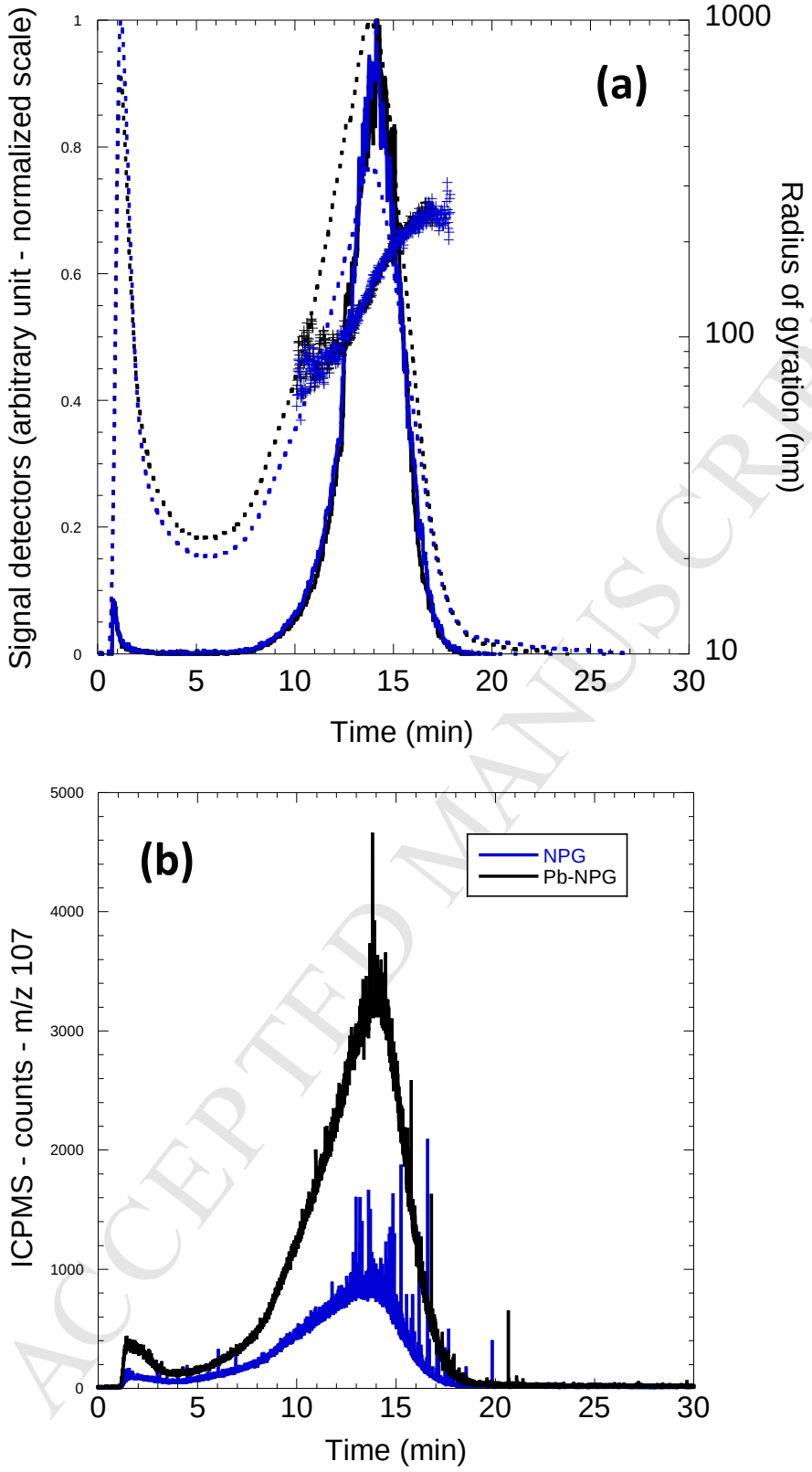

Figure 5: A4F fractograms of free Pb(II) and Pb(II)-doped NPG (a) the UV and SLS detection with the Rg variation (blue cross), (b) the ICP-MS detection with m/z ^{207}(Pb(II)).

Highlights

- Pb(II) binding experiments onto nanoplastics extracted from environmental micro-plastics were performed.
- Pb(II) was largely bound onto nanoplastics by specific adsorption and intra-particle diffusion.
- Nanoplastics could be significant vectors of metals in the environment